



A complementary strategy for producing moisture and alkane dual-responsive actuators based on graphene oxide and PDMS bimorph

Wei Wang^a, Yong-Lai Zhang^{a,*}, Bing Han^a, Jia-Nan Ma^a, Jian-Nan Wang^b, Dong-Dong Han^a, Zhuo-Chen Ma^b, Hong-Bo Sun^{a,b}

^a State Key Laboratory of Integrated Optoelectronics, College of Electronic Science and Engineering, Jilin University, 2699 Qianjin Street, Changchun 130012, China

^b State Key Laboratory of Precision Measurement Technology & Instruments, Department of Precision Instrument, Tsinghua University, Haidian district, Beijing 100084, China



ARTICLE INFO

Keywords:

Complementary strategy
Actuators
Dual-responsive
Graphene oxides
Bimorph

ABSTRACT

Smart actuators that enable deforming in a predictable manner under external stimuli have revealed great potential for both traditional and emerging industries. Generally, an asymmetric bilayer structure with one layer active and the other inert to a certain stimulus is essential to realize bending behavior. However, towards the development of dual- or multi-responsive actuators, it still lacks universal and effective strategies for rational design and fabrication of such devices through the simplest way. In this paper, we report a complementary strategy to produce dual-responsive bilayer actuators by combining the moisture-active/alkane-inert graphene oxide (GO) layer with the alkane-active/moisture-inert polydimethylsiloxane (PDMS) layer. The GO@PDMS bimorph actuator can switch its active and inert layers in response to moisture and alkane, respectively, realizing dual-responsive deformation under different actuations. Typical dual-responsive actuators, including a selective air valve and a grip and hook smart claw, are successfully fabricated, demonstrating the capability of effective gases and objects transmission. The complementary bimorph actuator may hold great promise for developing intelligent devices and portable delivery systems.

1. Introduction

Actuators that can convert various types of external stimuli into mechanical deformation are promising to perform mechanical work at various sizes. [1–4] Owing to the intelligent driving mechanisms and high sensitivity, smart actuators have been widely applied to both traditional and emerging industries, for example machinery [5–8], robotics [9–11], unmanned flight [12], sensors [13–17], in vivo surgery devices [18] and lab-on-a-chip systems [19–21]. Nowadays, various of energy sources such as magnetic field [20,22,23], light [24–29], heat [30–33], and humidity [34–37] have been successfully applied to trigger controllable movement of actuators. In general, actuators often adopt a bilayer structure, in which one layer is regarded as an active layer and the other is inert. The active layer changes its shape under external stimulus, while the inert layer remains unchanged. As a result, the bilayer actuator deforms in a controllable manner. As typical examples, Zhang et al. successfully proposed a series of moisture-driven bilayer actuators, which utilize graphene oxide (GO) as a humidity-active layer and reduced graphene oxide (RGO) as an inert layer [38]. Taccola et al. reported an electrostatic actuator consisting of PEDOT:

PSS and PDMS layers, where the PDMS acts an inert layer and PEDOT: PSS as an active layer [39]. Gracias et al. gave an example of graphene-polymer bilayers, realizing self-folded to form a completely integrated, curved, and folded structures under actuation. Herein, the polymer layer in the actuator functions as a solvent-active layer; and graphene serves as an inert layer [40]. Sun et al. successfully prepared a light-driven bilayer actuator composed of polydopamine-modified reduced graphene oxide (PDA-RGO) and (NOA)-63. The actuator possesses dual-responsive capability (light- and moisture-active), however, the active layer is merely PDA-RGO layer [41]. It is deserved to be noticed that all of the above-mentioned bilayer actuators only have one active layer. Sometimes, the active layer of some examples might be sensitive to two or more types of stimuli, leading to a dual-/multi-responsive actuation performance [42]. However, the adjustability and controllability of these actuators are highly hampered by their solo active-layer structures. In most cases, the inert layer that only acts as a restriction layer is not irreplaceable [43]. Towards the development of dual- or multi-responsive actuators, it is necessary to make full use of the bi-layers and simplify the device structures to the most extent. Currently, despite some pioneer works reported the multi-physical signals (e.g., light, heat

* Corresponding author.

E-mail address: yonglaizhang@jlu.edu.cn (Y.-L. Zhang).

<https://doi.org/10.1016/j.snb.2019.03.117>

Received 27 November 2018; Received in revised form 12 March 2019; Accepted 26 March 2019

Available online 28 March 2019

0925-4005/ © 2019 Published by Elsevier B.V.

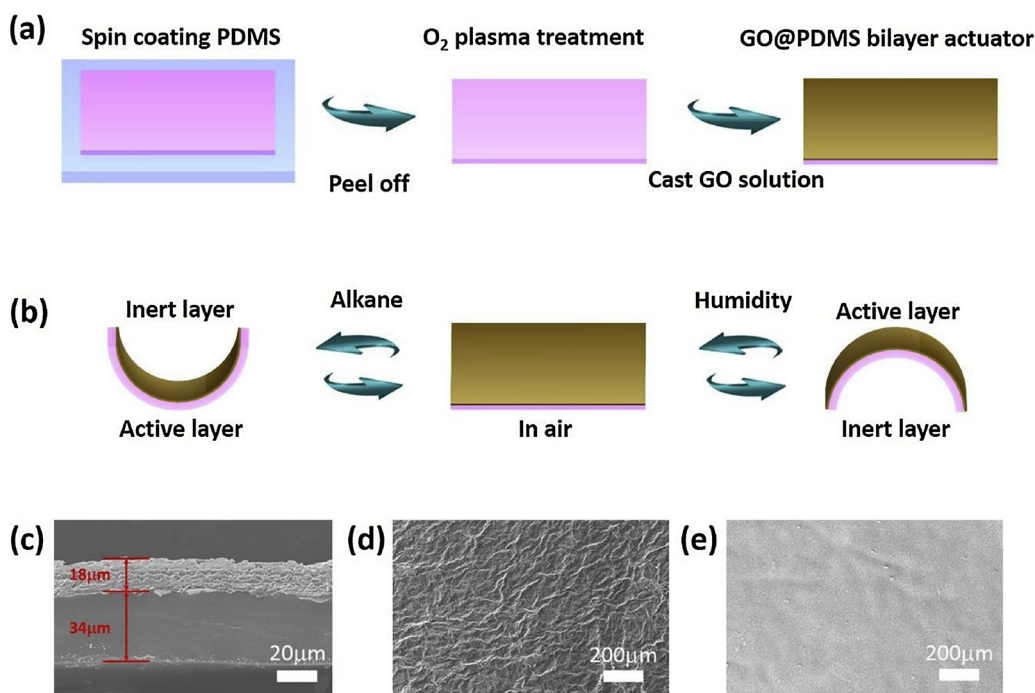


Fig. 1. Schematic illustration of the fabrication and working processes of the dual-responsive actuators based on GO and PDMS, including a) fabrication process, b) moisture/alkane-induced motion, and SEM image of c) the cross-section of bimorph actuator, d) the GO side of bimorph actuator, and e) the PDMS side of bimorph actuator.

and electricity) responsive actuators using different materials as active-layers [44–46], it is still rare to see the complementarity of inert and active layers under different chemical stimuli in the case of dual-responsive chemical actuators. In fact, a rational design of bilayer structure can lead to bidirectional deformation under distinct external stimuli. However, universal and effective strategies that can guide the design principle have not been reported yet.

Here, we report the production of a dual-responsive actuator with complementary active-inert layers using the complementary design principle. The moisture/alkane dual-responsive bimorph actuators are fabricated through simply combination of moisture-active/alkane-inert GO and alkane-active/moisture-inert polydimethylsiloxane (PDMS) bimorph. Under moisture actuation, GO layer expands due to the adsorption of water molecules, whereas the PDMS layer keeps unchanged. Accordingly, the GO@PDMS bilayer actuator bends towards the PDMS side. When the actuator is exposed to alkane, the PDMS layer becomes active; it swells due to the adsorption of alkane molecules, whereas the GO layer is inert, resulting in the reversed bending. In this way, dual-responsive GO@PDMS actuators, including a selective gas valve and a grip/hook smart claw, are successfully fabricated, demonstrating the capability gases and objects transmission. This rational complementary strategy may open up a new way for developing dual-responsive actuators.

2. Experiments

2.1. Preparation of GO@PDMS bimorph actuator

GO was obtained by modifying natural graphite powder (Aldrich, < 150 μm) with a modified Hummer's method. PDMS used in the devices was a commercially available PDMS elastomer (Sylgard 184 Silicone Elastomer, Dow Corning Corporation). Typically, the PDMS prepolymer was mixed with the curing agent with a ratio of 10:1 by weight.

The PDMS film was made through a spin-coating method (3000 rpm, 30 s), and then the film was cured at 95 °C for 30 min. After peeling off the PDMS film from the glass substrate, the PDMS membrane was treated with O₂ plasma for 3 min. Finally, the GO solution was cast onto the plasma-treated PDMS layer and dried naturally.

2.2. Characterization and measurement

Scanning electron microscopy (SEM) images were captured by a JEOL field-emission scanning electron microscope (JSM-7500). X-ray photoelectron spectroscopy (XPS) spectra were measured through an ESCALAB 250 spectrometer. Saturated salt solutions were used to create different relative humidity (RH) environment in the closed glass container ($P = 101.3 \text{ kPa}$, $T = 18 \pm 0.5 \text{ }^\circ\text{C}$). The saturated salt solutions of CH₃COOK, MgCl₂, K₂CO₃, NaBr, NaCl, and KCl, as well as pure H₂O were adopted (representing the RH = 23%, 33%, 44%, 57%, 75%, 86%, and 100%, respectively). All of the measurements were conducted in air at room temperature ($18 \pm 0.5 \text{ }^\circ\text{C}$). UV–vis transmittance spectra were measured by using a UV–vis spectrophotometer (UV-2550, SHIMADZU). X-ray diffraction (XRD) data were recorded by a Rigaku D/Max-2550 diffractometer with Cu K α radiation ($\lambda = 0.15418 \text{ nm}$). Raman spectra were measured on a JOBIN YVON T64000 instrument equipped with a liquid-nitrogen-cooled argon ion laser at 532 nm (Spectra-Physics Stabilite 2017) as an excitation source. The laser power was $\sim 30 \text{ } \mu\text{W}$ on the samples, and the average spot size was 1 μm in diameter using a long-working distance 50 \times objective.

3. Results and discussion

To realize the complementary strategy of alternating the active layer between bimorph, that is the inert layer and active layer can flexibly convert under different external stimuli, a simple O₂ plasma treatment and combination procedure was employed to make GO@PDMS bimorph actuators. According to PDMS and GO layer can swell in alkanes and humidity, respectively, such bilayer complementary devices are successfully prepared. Fig. 1a shows the fabrication procedure of the GO@PDMS bimorph actuator. PDMS was firstly spin-coated onto a glass substrate, followed by a high temperature curing (95 °C, 30 min). The PDMS membrane was then treated with O₂ plasma for 3 min [47]. The PDMS surface contained more oxygen-containing groups (OCGs) after plasma treatment; so that the combination of PDMS and GO was tight for long-time usage. The contact angle of the surface of PDMS membrane has changed greatly before and after O₂ plasma treatment (Fig. S1). Finally, GO solution was dropped onto PDMS membrane and drying naturally. The GO@PDMS bimorph actuator

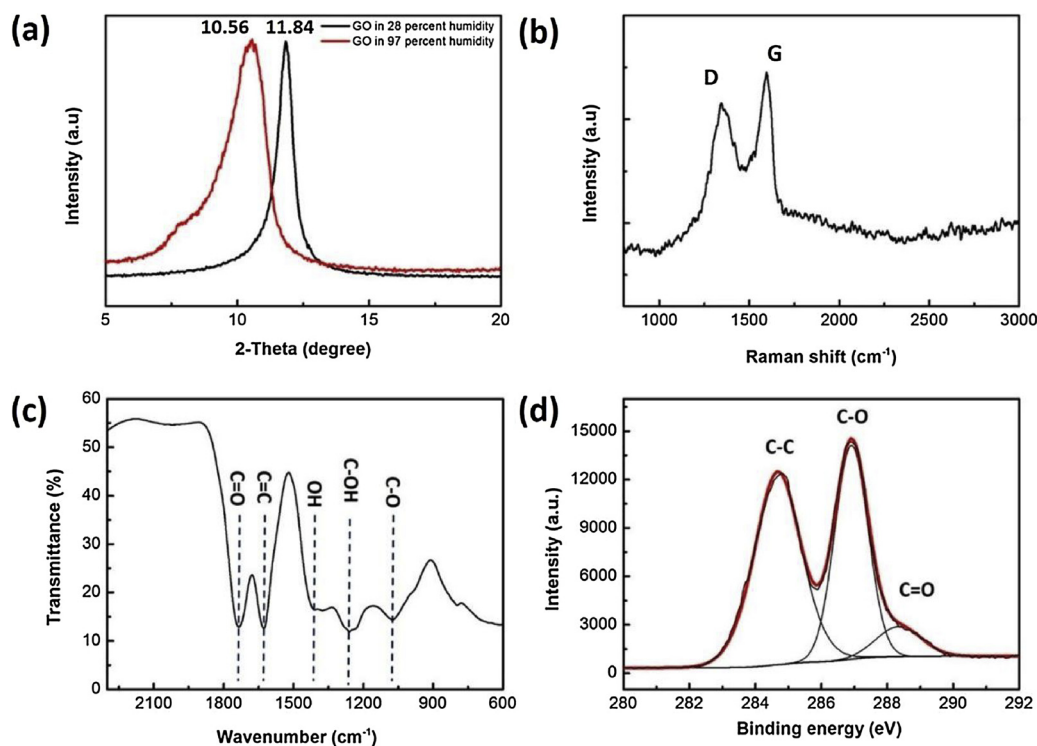


Fig. 2. a) XRD patterns of the GO side of the GO@PDMS bimorph actuator in the different RH. b) Raman spectra of the GO side of the GO@PDMS bimorph actuator. c) FTIR spectra of the GO side of the GO@PDMS bimorph actuator. d) C1s X-ray photoelectron spectroscopy (XPS) of the GO side of the GO@PDMS bimorph actuator.

enables flexible switching of inert and active layers, as illustrated in Fig. 1b. The actuator exhibited a relatively flat state in the air condition. When exposed to alkane, it gradually bends toward the GO side. In this process, the PDMS layer expands as an active layer and the GO layer acts as an inert layer with no volume change. However, when the actuator exposed to moisture, it bends to the PDMS side. In this case, the GO and PDMS switch the roles of inert and the active layers; the PDMS layer becomes inert, while the GO layer becomes active. Cross-section SEM image of the bilayer structure (Fig. 1c) reveals the thickness of GO layer and PDMS layer is $\sim 18\mu\text{m}$ and $\sim 34\mu\text{m}$, respectively. Fig. 1d-e illustrated the surface morphologies of GO and PDMS. There are more wrinkles on the surface of the GO layer, and the PDMS surface is relatively smooth.

Due to the abundance of OCGs, GO material is sensitive to humidity variation. As shown in Fig. 2a, XRD patterns showed that the layered structure of GO changed at various RH conditions (28% and 97%). The GO layer spacing increased along with the relative humidity, since the typically diffraction peak at $2\theta = 11.84^\circ$ (RH = 28%) changed to $2\theta = 10.56^\circ$ (RH = 97%), corresponding to the d-spacing of GO layer changed from 0.75 nm to 0.84 nm. Such significant increment of the GO interlayer spacing is confirmed at higher RH condition. From the macroscopic perspective, GO swells under moisture treatment [48,49]. However, no significant swelling occurred when GO was immersed in n-Hexane for 265 s, as shown in Fig. S2.

Characterization of carbon materials by Raman spectroscopy is a convincing way. Clearly, the two distinct peaks at 1329 and 1589 cm^{-1} represented the D and G bands, respectively (Fig. 2b). The G band is characteristic of sp^2 carbons, while the D band is related to the breathing modes of the graphitic domains and the existence of defects. The OCGs on the GO surface presents an important role in combining with water molecules. In our measurement, Fourier transform infrared (FTIR) spectra (Fig. 2c) have been applied to measure the oxygen groups of GO. Notably, GO showed abundant aggregation of transmission bands corresponding to OCGs (e.g., C=O at 1724 cm^{-1} , C–O at 1039 cm^{-1}). The chemical composition of GO is further studied by XPS

(Fig. 2d). The C1s spectra can be resolved into three peaks. Notably, the peaks at 288.3, 286.9, and 284.7 eV are attributed to C=O (carbonyl), C–O (hydroxyl and epoxy carbon) and C–C (non-oxygenated ring carbon), respectively. The results showed that the highest intensity at the peak of 286.9 eV, indicating the GO layer has a better oxidation degree.

Theoretically, PDMS have a swelling effect when it encountered hydrocarbons. We further verified this theory by experiments. In the experiment, n-hexane was selected as the stimulus and recorded video to observe the changes of PDMS before and after encountering with n-hexane. As shown in Fig. 3a, a square block of PDMS doped with R6G with the length and width of 2 cm was prepared in the air. Then the PDMS film was put into a container, which was filled with n-hexane, the PDMS expanded rapidly. The length and width of PDMS block expand to ~ 2.3 cm after 263 s (Fig. 3b). However, no significant swelling performance occurred when PDMS square block was immersed in water for 242 s as shown in Fig. S3. The above experiment proves that the swelling effect of PDMS layer when it is encountered by n-hexane, so that the PDMS can be used as the active layer of the actuator when n-hexane acts as a stimulus source.

In addition to n-hexane, PDMS also has similar swelling effect in response to other organic vapors. To prove the universal responsiveness to other organic vapors, the actuators ($1.0\text{ mm} \times 15.0\text{ mm}$) was tested in six kinds of vapor environments, including n-heptane, n-pentane, n-hexane, toluene, acetone and benzene, respectively (Fig. 4a). The results show that the actuators generally bend in response to all of the organic vapors. Especially, under the actuation of alkanes vapor, the bending curvature is much larger, as shown in the insets of Fig. 4a. Interestingly, the GO@PDMS bimorph actuator also shows obvious moisture-responsive properties due to the strong expansion ability of the GO in humidity. To quantitatively investigated their actuation performance, the curvature of a GO@PDMS ribbon ($1.0\text{ mm} \times 15.0\text{ mm}$) under different RH was measured (Fig. 4b). With the increase of RH from 23% to 100%, the bending curvature of the GO@PDMS ribbon gradually increased from 2.4 cm^{-1} to 10 cm^{-1} . The insets of Fig. 4b are

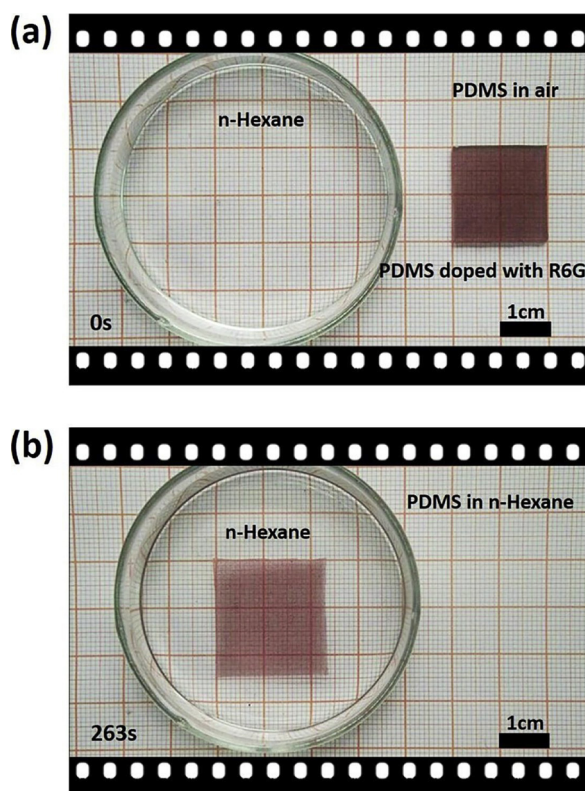


Fig. 3. Swelling effect of PDMS in n-Hexane. a) PDMS doped with R6G in air without swelling. b) PDMS doped with R6G in n-Hexane with significant swelling.

photographs of the ribbon under different RHs. The RH greatly influences the bending performance of GO@PDMS bimorph, where the GO layer is active. To reach the best potential of actuators, appropriate RH must be taken into consideration.

However, due to the bimorph actuator enables mutual conversion between the active and inert layers, so the relative thickness of the two layers is crucial. In order to explore the influence of the bilayer thicknesses on actuation, the following studies were conducted. As shown in Fig. 5a, actuators with different thicknesses of the GO layer (from 4.3 to 20 μm) were made, while the thickness of PDMS layer remains 34 μm . The curvature of actuators varied from 6.5 to 11 cm^{-1} under RH = 100%. When the actuators were put into the n-hexane, these actuators' curvature changed from -33.7 to -12.4 cm^{-1} . This phenomenon can be explained as that GO is active layer under humidity stimulus, the interlayer distance of GO sheet within the material expanded as a function of RH. So that the bending curvature increases along with the thickness of GO layer, On the contrary, GO act as an inert layer in n-Hexane. GO constraint the volume change of PDMS, therefore the curvature reduces along with the increment of GO layer. Since PDMS and GO membranes serve as a complement active/inert layer in the bimorph actuator, the thickness of PDMS effects the curvature completely reversed, as shown in Fig. 5b. Samples with different thicknesses of the PDMS layer (from 34 to 277 μm) were prepared. The bending curvature changed from 11 to 2.9 cm^{-1} , where the thickness of GO layer remained unchanged (20 μm) under 100% RH. Moreover, the curvature changed from -12.4 to -45 cm^{-1} under the situation of n-hexane stimulus. Briefly, the bending curvature of actuator becomes larger in n-Hexane and becomes smaller in moisture when the thickness of PDMS layer is gradually increased, because of the PDMS function as active layer or inert layer, respectively.

To make a clear overview of the responsiveness of these bimorph actuators under different stimuli, we evaluated the dependence of bending curvatures under moisture and alkane actuation on the PDMS/

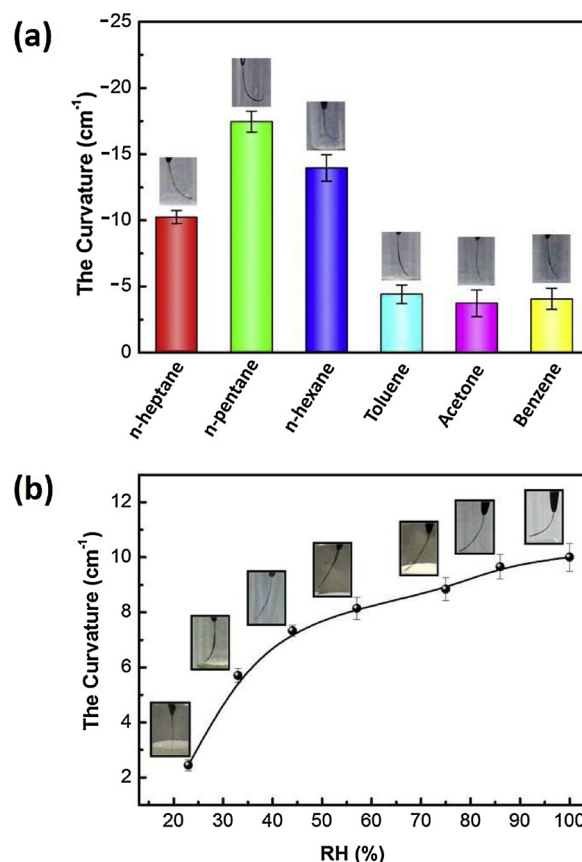


Fig. 4. a) The dependence of the curvature of the GO@PDMS bimorph actuator on different organic gases. The insets are photographs of GO@PDMS bimorph actuator under the actuation of different organic vapors. b) The dependence of the curvature of the GO@PDMS bimorph actuator on RH. The insets are photographs of GO@PDMS bimorph actuator under different humidity.

GO thickness ratios (Fig. 5c). In response to moisture, the bending curvature decreased with the increase of the PDMS/GO thickness ratios; whereas under alkane actuation, the responsiveness tendency is contrary. To make a trade-off between moisture and alkane responsiveness, the PDMS/GO thickness should be ~ 2 .

To verify the stability and the response recovery time of the bimorph actuator, actuators adopted in the following research are unified with GO and PDMS thicknesses of 18 μm and 34 μm , respectively. The actuation performances of GO@PDMS actuators in n-Hexane and moisture are characterized for three cycles (Fig. 6). In the n-Hexane triggered experiment, the actuator takes 16 s to reach maximum bending curvature (~ 14 cm^{-1}) and takes ~ 7 s to recover to the initial state. During three bending cycles, the actuator shows good reversibility and stability. When triggered by moisture (RH from 28% to 97%), the actuator takes ~ 7 s for bending and ~ 14 s for recovery (Fig. 6b). The GO@PDMS bimorph actuator is relatively stable in terms of bending curvature and response/recovery time in both n-Hexane and moisture treatments.

The rational design of smart bimorph actuators based on GO@PDMS membranes enables unique inert and active layer complementary exchange. We develop a smart air valve model to illustrate the selective transportation of different gas. Six GO@PDMS bimorph actuators (2.0 mm \times 12.0 mm) were put right on six air holes (2.0 mm \times 10 mm) with one end fixed on the substrate, as shown in Fig. 7. Herein, the PDMS layer faced up and the GO layer faced down. At the initial state the bimorph actuator remained flat, when there was no n-hexane and water vapor. When treated with moisture, the GO layer became active and the actuator bent upwards. Thereby, the air valve opened allowing moisture pass through. It took 7 s for the actuators to open up. Then the

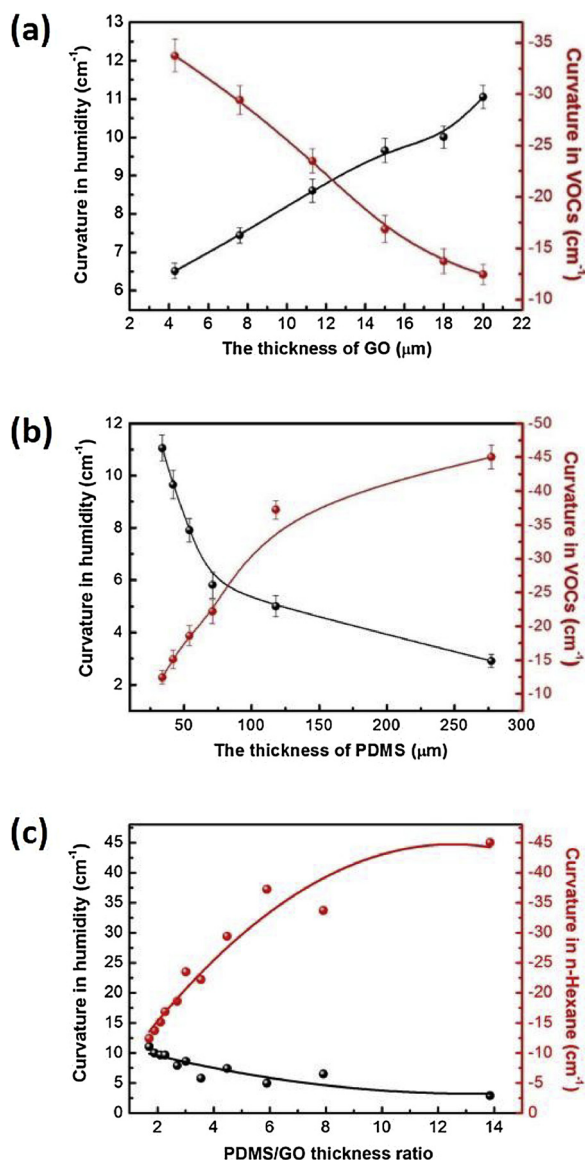


Fig. 5. The dependence of the curvature of the GO@PDMS bimorph actuator on thickness of each layer under humidity or n-Hexane. a) The dependence of the curvature on thickness of GO layer. b) The dependence of the curvature on thickness of PDMS layer. c) The dependence of the responsiveness under moisture and alkane actuation on the PDMS/GO thickness ratio.

moisture treatment was stopped and n-hexane vapor was presented, the PDMS layer expanded due to the swelling effect. At this time, the GO layer returned to the initial state, which means the actuator bent downwards. Since the size of the vent hole is smaller than the actuators, the valves were firmly closed. This phenomenon can prevent the leakage of n-hexane vapors, the entire process lasted 32 s. We can reversely utilize the bimorph as an n-hexane-selective valve, to allow n-hexane pass through and block the passage of moisture, as shown in Fig. 7b. We just put the GO@PDMS actuators upside down. When the n-hexane vapor was present, PDMS layer expanded and the actuator bent upwards to open the vent holes allowing n-hexane vapor to pass through. It took 21 s for the actuator to reach the stable state. When the n-hexane vapor was removed and the moisture treatment was presented, the PDMS layer returned to the initial state. Resulting in the actuator bent downwards to close the vent holes and prevent the leakage of moisture. The entire process lasted for 26 s. The smart unidirectional transmission vent has successfully achieved to the control of gas transmission.

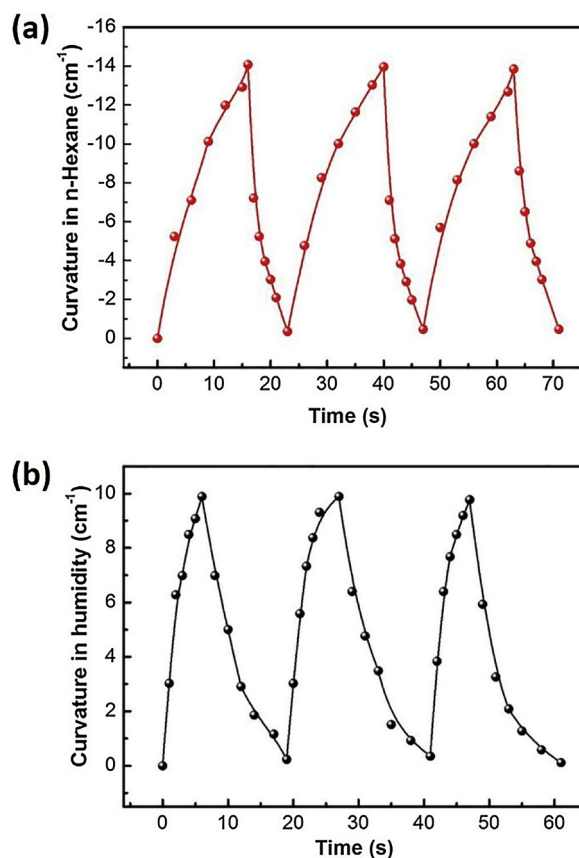


Fig. 6. Responsive and recovery properties of the GO@PDMS bimorph actuator. RH was switched between 28% and 97% three times. a) Repeated response of the GO@PDMS bimorph actuator in n-hexane vapors. b) Repeated response of the GO@PDMS bimorph actuator in humidity.

The actuator can not only control the transmission of the gas, but also can realize the pick and transport of objects. As shown in Fig. 8, with the aid of the microfluidic channels, the actuator can realize functions of the claws and the hooks by switching between the inert layer and the active layer. Fig. 8a illustrates the design mechanism of this smart actuator. A thick tube was used as a humidity channel, and evenly distributed three thin tubes as n-Hexane channels. The GO@PDMS bimorph actuators ($1.0 \text{ mm} \times 15.0 \text{ mm}$) were pasted onto the bottom of the thick tube. Two kinds of objects were placed on the substrate that can be grabbed and hooked separately (Fig. 8b). Firstly, the smart actuator was placed above the white block, as shown in Fig. 8c. Then we slowly moved it right below the actuator. As moisture is passed in from the humidity channel, the GO layer expanded and the bimorph bent inwards, which function as claws, so that the white block object can be successfully grabbed (Fig. 8d). Subsequently, stopped the input of humidity, the claws are recovered to the initial state and put the object down. Then the smart actuator is moved right over the three square rings. Interestingly, with the aid of the microfluidic device, the n-hexane was injected through the n-hexane channel. Once the PDMS layer is exposed to n-hexane, it expanded rapidly, so that the bimorph bent outwards just like hooks. The three rings can be successfully hooked up as shown in Fig. 8f. The entire process lasted for 76 s. The above experiments successfully demonstrated that the GO@PDMS bimorph actuator enables the transmission of gas and objects. These results also indicate that the dual-responsive actuator with complementary strategy based on GO and PDMS bimorph holds great promise for developing intelligent actuators. Furthermore, considering the fact that the manipulation of such actuators could be achieved without any coupled energy-supply systems, the dual-responsive GO@PDMS bimorph may find broad applications in intelligent devices, for

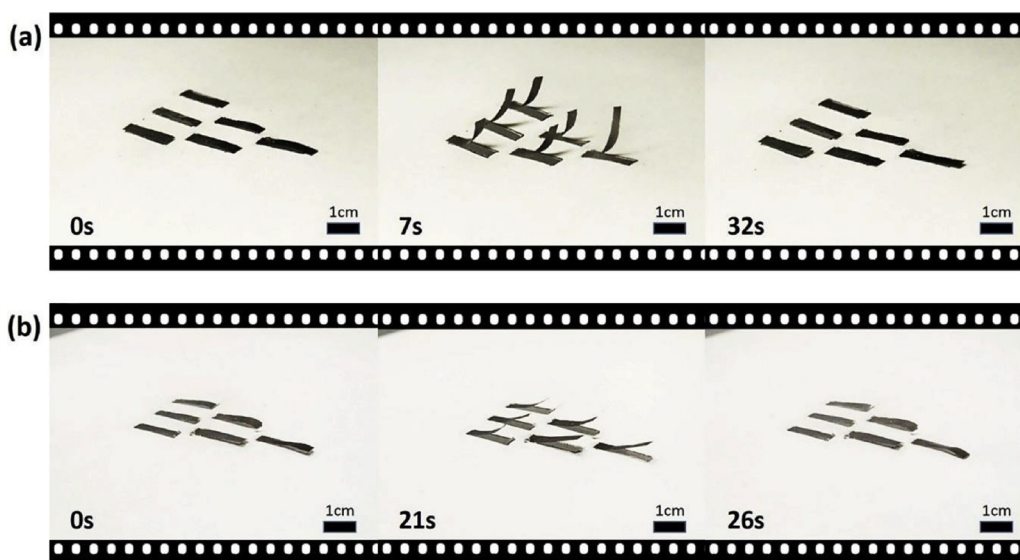


Fig. 7. The dual-responsive performance of a selective air valve. a) The selective air valve could bend upwards when treated with moisture, the GO layer became active and allowed moisture transmission, however it will be closed with increasing n-hexane concentration and the entire process lasted 32 s. b) When the actuator was reversed, it was bent upwards when n-hexane was presented allowing n-hexane pass through, however it will be closed with increasing moisture concentration and the entire process lasted 26 s. See Videos S1 and S2 of the Supporting Information.

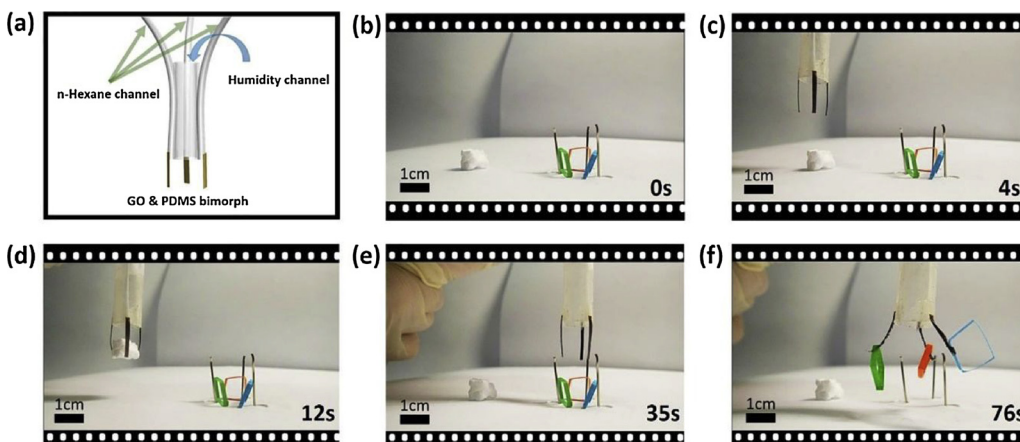


Fig. 8. Taking advantages of alternate the active layer of bilayer actuator, an intelligent hook smart claw was prepared with the aid of a microfluidic chip. a) Schematic illustration of the intelligent actuator. (b)-(d) The actuator functions as claws to grasp and drop the object with change of RH. (e)-(f) With the outflow of n-hexane liquid, the actuator works as hooks to hook up objects. See Videos S3 of the Supporting Information.

instance, smart textiles, sensors, and even tissue engineering.

4. Conclusions

In conclusion, a rational complementary strategy to alternate the active layer of bilayer actuator by a simple combination of the moisture-active GO layer and the alkane-active PDMS layer is achieved. Due to the rational design that actuator can realize flexible switching of its own inert and active layer in the presence of moisture or alkanes based on GO and PDMS bimorph. The smart bimorph actuator was very sensitive to moisture and alkane; GO is a moisture-active material, on the contrary, the PDMS is insensitive to moisture. In this case, the GO@PDMS bilayer actuator bends towards the PDMS side with respect to the moisture treatment. When the actuator is exposed to alkane, the situation is reversed. The PDMS layer acts as the active layer and the GO layer becomes the inert layer, resulting in a bending performance towards the GO side. To get better control over the responsive characteristics of the actuator, GO@PDMS actuator with a certain curvature rely on various thickness of GO and PDMS have been successfully prepared. Furthermore, typical applications of these actuators, including a selective air valve and a grip and hook smart claw are designed and fabricated, indicating the effective transmission of gases and objects. Briefly, a simple, effective fabrication method of combining two materials which can respond to different energy sources shows unique merits for designing bilayer actuators with rational complementary strategy. The switchable property of the active and inert

layers makes actuators hold great promise for the development of multiple-responsive smart robots.

Acknowledgments

The authors acknowledge the National Key Research and Development Program of China and National Natural Science Foundation of China under Grants #2017YFB1104300, #61775078, #61590930, and #61605055 for support. We also acknowledge the Natural Science Foundation of Jilin Province Nos. #20180101061JC.

Appendix A. Supplementary data

Supplementary material related to this article can be found, in the online version, at doi:<https://doi.org/10.1016/j.snb.2019.03.117>.

References

- [1] J. Zhang, L. Song, Z.P. Zhang, N. Chen, L.T. Qu, Environmentally responsive graphene systems, *Small* 10 (2014) 2151–2164.
- [2] Y. Zhao, Q. Han, Z.H. Cheng, L. Jiang, L.T. Qu, Integrated graphene systems by laser irradiation for advanced devices, *Nano Today* 12 (2017) 14–30.
- [3] J.-N. Wang, Y.-Q. Liu, Y.-L. Zhang, J. Feng, H. Wang, Y.-H. Yu, et al., Wearable superhydrophobic elastomer skin with switchable wettability, *Adv. Funct. Mater.* 28 (2018) 1800625.
- [4] Y. Kim, M. Han, J. Kim, E. Kim, Electrochromic capacitive windows based on all conjugated polymers for a dual function smart window, *Energy Environ. Sci.* 11 (2018) 2124–2133.
- [5] C. Maggi, F. Saglimbeni, M. Dipalo, F. De Angelis, R. Di Leonardo, *Micromotors*

- with asymmetric shape that efficiently convert light into work by thermocapillary effects, *Nat. Commun.* 6 (2015) 7855.
- [6] Y. Hu, Z. Li, T. Lan, W. Chen, Photoactuators for direct optical-to-mechanical energy conversion: from nanocomponent assembly to macroscopic deformation, *Adv. Mater.* 28 (2016) 10548–10556.
- [7] W. Wang, Y.Q. Liu, Y. Liu, B. Han, H. Wang, D.D. Han, et al., Direct laser writing of superhydrophobic PDMS elastomers for controllable manipulation via marangoni effect, *Adv. Funct. Mater.* 27 (2017) 1702946.
- [8] Y. Zhao, B. Xu, G. Zheng, J. Zheng, X. Qiu, M. Zhuang, et al., Improving the performance of IPMCs with a gradient in thickness, *Smart Mater. Struct.* 22 (2013) 5035.
- [9] T. Petit, L. Zhang, K.E. Peyer, B.E. Kratochvil, B.J. Nelson, Selective trapping and manipulation of microscale objects using mobile microvortices, *Nano Lett.* 12 (2012) 156.
- [10] M.J. Villangca, D. Palima, A.R. Bañas, J. Glückstad, Light-driven micro-tool equipped with a syringe function, *Light Sci. Appl.* 5 (2016) e16148.
- [11] Y. Wang, X. Chen, K. Sun, K. Li, F. Zhang, B. Dai, et al., Directional transport of centi-scale object on anisotropic microcilia surface under water, *Sci. China Mater.* (2018) 1–9.
- [12] S.M. Azizi, K. Khorasani, Cooperative actuator fault accommodation in formation flight of unmanned vehicles using relative measurements, *Control Theory Appl. Iet* 84 (2011) 876–894.
- [13] D. Kastor, S. Ray, J. Traschen, Sensors and actuators based on surface acoustic waves propagating along solid–liquid interfaces, *J. Phys. D Appl. Phys.* 41 (2008) 123002.
- [14] O.A. Aramori, S. Rosset, H.R. Shea, High-Resolution, Large-area fabrication of compliant electrodes via laser ablation for robust, stretchable dielectric elastomer actuators and sensors, *ACS Appl. Mater. Interfaces* 7 (2015) 18046.
- [15] B. Yang, W.T. Bi, C.A. Zhong, M.C. Huang, Y. Ni, L.H. He, et al., Moisture-triggered actuator and detector with high-performance: interface engineering of graphene oxide/ethyl cellulose, *Sci. China-Mater.* 61 (2018) 1291–1296.
- [16] G. Wissmeyer, M.A. Pleitez, A. Rosenthal, V. Ntziachristos, Looking at sound: optoacoustics with all-optical ultrasound detection, *Light-Sci. Appl.* 7 (2018) 53.
- [17] Q.M. Ji, I. Honma, S.M. Paek, M. Akada, J.P. Hill, A. Vinu, et al., Layer-by-layer films of graphene and ionic liquids for highly selective gas sensing, *Angew. Chem.-Int. Edit* 49 (2010) 9737–9739.
- [18] Z. Li, P. Tristan, L. Yang, B.E. Kratochvil, K.E. Peyer, P. Ryan, et al., Controlled propulsion and cargo transport of rotating nickel nanowires near a patterned solid surface, *ACS Nano* 4 (2010) 6228.
- [19] L. Zhang, K.E. Peyer, B.J. Nelson, Artificial bacterial flagella for micromanipulation, *Lab Chip* 10 (2010) 2203–2215.
- [20] Y. Tian, Y.L. Zhang, J.F. Ku, Y. He, B.B. Xu, Q.D. Chen, et al., High performance magnetically controllable microturbines, *Lab Chip* 10 (2010) 2902–2905.
- [21] Y.S. Zeng, H. Fan, B. Xu, Z. Zhang, F.F. Ren, C. Zhou, et al., A facile strategy to integrate robust porous aluminum foil into microfluidic chip for sorting particles, *Microfluid. Nanofluidics* 21 (2017) 173.
- [22] S. Kim, S. Lee, J. Lee, B.J. Nelson, L. Zhang, H. Choi, Fabrication and manipulation of ciliary microrobots with non-reciprocal magnetic actuation, *Sci. Rep.* 6 (2016) 30713.
- [23] T. Xu, J. Yu, X. Yan, H. Choi, L. Zhang, Magnetic actuation based motion control for microrobots: an overview, *Micromachines* 6 (2015) 1346–1364.
- [24] K. Kumar, C. Knie, D. Bléger, M.A. Peletier, H. Friedrich, S. Hecht, et al., A chaotic self-oscillating sunlight-driven polymer actuator, *Nat. Commun.* 7 (2016) 11975.
- [25] D. Okawa, S.J. Pastine, A. Zettl, J.M. Fréchet, Surface tension mediated conversion of light to work, *J. Am. Chem. Soc.* 131 (2009) 5396.
- [26] Y. Zhao, L. Song, Z. Zhang, L. Qu, Stimulus-responsive graphene systems towards actuator applications, *Energy Environ. Sci.* 6 (2013) 3520–3536.
- [27] D. Gao, W. Ding, M. Nietovesperinas, X. Ding, M. Rahman, T. Zhang, et al., Optical manipulation from the microscale to the nanoscale: fundamentals, advances and prospects, *Light Sci. Appl.* 6 (2017) e17039.
- [28] D.D. Han, Y.L. Zhang, J.N. Ma, Y.Q. Liu, B. Han, H.B. Sun, Light-mediated manufacture and manipulation of actuators, *Adv. Mater.* 28 (2016) 8328–8343.
- [29] L. Jiang, A.D. Wang, B. Li, T.H. Cui, Y.F. Lu, Electrons dynamics control by shaping femtosecond laser pulses in micro/nanofabrication: modeling, method, measurement and application, *Light Sci. Appl.* 7 (2018) 17134.
- [30] P. Virgil, M.R. Imam, P. Mihai, L. Pawaret, Self-organizable vesicular columns assembled from polymers dendronized with semifluorinated janus dendrimers act as reverse thermal actuators, *J. Am. Chem. Soc.* 134 (2012) 4408.
- [31] B. Han, Y.L. Zhang, Q.D. Chen, H.B. Sun, Carbon-based photothermal actuators, *Adv. Funct. Mater.* 28 (2018) 1802235.
- [32] W. Zhang, H. Zappe, A. Seifert, Wafer-scale fabricated thermo-pneumatically tunable microlenses, *Light Sci. Appl.* 3 (2014) e145.
- [33] J. Na, J.S. Heo, M. Han, H. Lim, H.O. Kim, E. Kim, Harvesting of living cell sheets by the dynamic generation of diffractive photothermal pattern on PEDOT, *Adv. Funct. Mater.* 27 (2017) 1604260.
- [34] G. Wang, H. Xia, X.C. Sun, C. Lv, S.X. Li, B. Han, et al., Actuator and generator based on moisture-responsive PEDOT: PSS/PVDF composite film, *Sens. Actuator B-Chem.* 255 (2018) 1415–1421.
- [35] D.D. Han, Y.L. Zhang, Y. Liu, Y.Q. Liu, H.B. Jiang, B. Han, et al., Bioinspired graphene actuators prepared by unilateral UV irradiation of graphene oxide papers, *Adv. Funct. Mater.* 25 (2015) 4548–4557.
- [36] C. Huhu, H. Yue, Z. Fei, D. Zelin, W. Yanhong, C. Nan, et al., Moisture-activated torsional graphene-fiber motor, *Adv. Mater.* 26 (2014) 2909–2913.
- [37] V. Manikandan, I. Petrilă, S. Vignesvelan, R. Dharmavarapu, S. Juodkazis, S. Kavita, et al., Efficient humidity-sensitive electrical response of annealed lithium substituted nickel ferrite (Li-NiFe₂O₄) nanoparticles under ideal, real and corrosive environments, *J. Mater. Sci.-Mater. Electron* 29 (2018) 18660–18667.
- [38] D.D. Han, Y.L. Zhang, H.B. Jiang, H. Xia, J. Feng, Q.D. Chen, et al., Graphene: moisture-responsive graphene paper prepared by self-controlled photoreduction, *Adv. Mater.* 27 (2015) 332–338.
- [39] T. Silvia, G. Francesco, S. Edoardo, M. Alessio, M. Barbara, M. Virgilio, Toward a new generation of electrically controllable hygromorphic soft actuators, *Adv. Mater.* 27 (2015) 1668–1675.
- [40] T. Deng, C.K. Yoon, Q. Jin, M. Li, Z. Liu, D.H. Gracias, Self-folding graphene-polymer bilayers, *Appl. Phys. Lett.* 106 (2015) 183.
- [41] M. Ji, N. Jiang, J. Chang, J. Sun, Near-infrared light-driven, highly efficient bilayer actuators based on polydopamine-modified reduced graphene oxide, *Adv. Funct. Mater.* 24 (2015) 5412–5419.
- [42] L. Chen, M. Weng, F. Huang, W. Zhang, Light- and humidity-driven actuators with programmable complex shape-deformations, *Sens. Actuators B Chem.* 282 (2019) 384–390.
- [43] E. Sacyani, M. Layani, G. Tibi, T. Avidan, A. Degani, S. Magdassi, Enhanced movement of CNT-based actuators by a three-layered structure with controlled resistivity, *Sens. Actuators B Chem.* 252 (2017) 1071–1077.
- [44] W. Wang, C. Xiang, Q. Zhu, W. Zhong, M. Li, K. Yan, et al., Multistimulus responsive actuator with GO and carbon nanotube/PDMS bilayer structure for flexible and smart devices, *ACS Appl. Mater. Interfaces* 10 (2018) 27215–27223.
- [45] L. Chen, M. Weng, P. Zhou, L. Zhang, Z. Huang, W. Zhang, Multi-responsive actuators based on a graphene oxide composite: intelligent robot and bioinspired applications, *Nanoscale* 9 (2017) 9825–9833.
- [46] Y. Jiang, C.G. Hu, H.H. Cheng, C.X. Li, T. Xu, Y. Zhao, et al., Spontaneous, straightforward fabrication of partially reduced graphene oxide-polyppyrrrole composite films for versatile actuators, *ACS Nano* 10 (2016) 4735–4741.
- [47] J.N. Wang, Y.Q. Liu, Y.L. Zhang, J. Feng, H.B. Sun, Pneumatic smart surfaces with rapidly switchable dominant and latent superhydrophobicity, *NPG Asia Mater.* 10 (2018) e470.
- [48] R.R. Nair, H.A. Wu, P.N. Jayaram, I.V. Grigorieva, A.K. Geim, Unimpeded permeation of water through helium-leak-tight graphene-based membranes, *Science* 335 (2012) 442–444.
- [49] C. Huhu, L. Jia, Z. Yang, H. Chuangang, Z. Zhipan, C. Nan, et al., Graphene fibers with predetermined deformation as moisture-triggered actuators and robots, *Angew. Chem.* 125 (2013) 10676–10680.

Wei Wang is currently pursuing his Ph.D. at Jilin University, China. His research interests include functional actuators based on carbon materials and laser additive manufacturing.

Yong-Lai Zhang received his BSc (2004) and PhD (2009) from Jilin University, China. He joined Jilin University in 2010 and is currently a full professor in the State Key Laboratory on Integrated Optoelectronics, College of Electronic Science and Engineering, Jilin University. In 2011, he was awarded a “Hong Kong Scholar” postdoctoral fellow. His research interests include laser fabrication, graphene-based microdevices, smart robotics and Lab-on-a-Chip systems.

Bing Han is currently pursuing her Ph.D. at Jilin University, China. Her research interests include laser printed graphene devices, applications of graphene materials in optical detection, and light-driven bio-inspired robots.

Jia-Nan Ma is currently pursuing her Ph.D. at Jilin University, China. Her research interests include intelligent actuator based on graphene.

Jian-Nan Wang received her Ph.D. degree in microelectronics and solid electronics from Jilin University (China) in 2018. She is currently working as a postdoctoral researcher at Tsinghua University. Her research interest focuses on micronanofabrication of smart surfaces.

Dong-Dong Han received his B.S. degree from College of Electronic Science and Engineering, Jilin University, China. He is now pursuing his Ph.D. at Jilin University, China. Currently his research interests mainly include graphene-based sensors and actuators.

Zhuo-Chen Ma received his PhD degree in Electronic Science and Engineering from Jilin University, China, in 2016. He is currently a postdoctoral at Tsinghua University. His research interests include femtosecond laser nanofabrication and metallic micro/nanostructures.

Hong-Bo Sun received the B.S. and the Ph.D. degrees in electronics from Jilin University, China, in 1992 and 1996, respectively. He worked as a postdoctoral researcher in Satellite Venture Business Laboratory, the University of Tokushima, Japan, from 1996 to 2000, and then as an assistant professor in Department of Applied Physics, Osaka University, Osaka, Japan. In 2005, he was promoted as a full professor (Changjiang Scholar) in Jilin University, China. In 2017, he moved to Department of Precision Instrument, Tsinghua University, China. His research interests have been focused on ultrafast laser nanofabrication of various micro-optical, microelectronic, micromechanical, micro-optoelectronic, microfluidic components and their integrated systems at nanoscale.